Geol. Mag. **154** (*6*), *2017, pp. 1344–1359.* © *Cambridge University Press 2017*
doi:10.1017/S0016756817000115

Marine redox evolution in the early Cambrian Yangtze shelf margin area: evidence from trace elements, nitrogen and sulphur isotopes

GUANG-YI WEI*, HONG-FEI LING*†, DA LI*, WEI WEI*, DAN WANG‡, XI CHEN*, XIANG-KUN ZHU‡, FEI-FEI ZHANG§ & BIN YAN‡

*State Key Laboratory for Mineral Deposits Research, School of Earth Science and Engineering, Nanjing University, Nanjing 210023, China
‡MLR Key Laboratory of Isotope Geology, State Key Laboratories of Continental Tectonics and Dynamics, Institute of Geology, Chinese Academy of Geological Sciences, Beijing 100037, China
§School of Earth and Space Exploration, Arizona State University, Tempe, AZ 85287-6004, USA

(*Received* 23 June 2016; *accepted* 7 February 2017; *first published online* 22 March 2017)

Abstract – Nitrogen is an essential element for biological activity, and nitrogen isotopic compositions of geological samples record information about both marine biological processes and environmental evolution. However, only a few studies of N isotopes in the early Cambrian have been published. In this study, we analysed nitrogen isotopic compositions, as well as trace elements and sulphur isotopic compositions of cherts, black shales, carbonaceous shales and argillaceous carbonates from the Daotuo drill core in Songtao County, NE Guizhou Province, China, to reconstruct the marine redox environment of both deep and surface seawater in the study area of the Yangtze shelf margin in the early Cambrian. The Mo–U covariation pattern of the studied samples indicates that the Yangtze shelf margin area was weakly restricted and connected to the open ocean through shallow water flows. Mo and U concentrations, $\delta^{15}N_{bulk}$ and $\delta^{34}S_{py}$ values of the studied samples from the Yangtze shelf margin area suggest ferruginous but not sulphidic seawater and low marine sulphate concentration (relatively deep chemocline) in the Cambrian Fortunian and early Stage 2; sulphidic conditions (shallow chemocline and anoxic photic zone) in the upper Cambrian Stage 2 and lower Stage 3; and the depression of sulphidic seawater in the middle and upper Cambrian Stage 3. Furthermore, the decreasing $\delta^{15}N$ values indicate shrinking of the marine nitrate reservoir during the middle and upper Stage 3, which reflects a falling oxygenation level in this period. The environmental evolution was probably controlled by the changing biological activity through its feedback on the local marine environment.

Keywords: Yangtze shelf margin, early Cambrian, local redox condition, nitrogen cycle, biological feedback

1. Introduction

The Ediacaran–Cambrian (E-C) transition (635–520 Ma) is an important period in Earth history that witnessed the rise of marine oxygen content and the Cambrian Explosion of life (Li *et al.* 2008; Och & Shields-Zhou, 2012; Shields-Zhou & Zhu, 2013; Lyons, Reinhard & Planavsky, 2014; Chen *et al.* 2015). Biological evolution may have been triggered by environmental changes and may also have affected the environment. Many studies have reported changes in both life and environment during this period and many geochemical indices are used in studies of marine environmental change, such as trace elements, rare earth elements, iron speciation, and isotopes of sulphur and molybdenum (Goldberg, Poulton & Strauss, 2005; Lyons *et al.* 2009; Li *et al.* 2010; Ling *et al.* 2013; Och *et al.* 2013; Chen *et al.* 2015; Cheng *et al.* 2016). In South China, many typical marine sediment sections are exposed, from platform to slope to deep basin, in the Nanhua Basin during the Ediacaran–Cambrian transition, with various lithologies, such as carbonates, siliceous rocks and black shales. By studying some of these sections and other coeval sections in the world, several researchers concluded that the ocean became highly oxygenated in the terminal Neoproterozoic through pulses of oxygen increase in the ocean (Fike *et al.* 2006; Canfield *et al.* 2007;); meanwhile, other researchers obtained evidence for anoxic or ferruginous seawaters, or even a euxinic environment in the shelf margin area of the Yangtze Block, South China, during the Ediacaran–Cambrian transition (Steiner *et al.* 2001; Goldberg *et al.* 2007; Li *et al.* 2010, 2012; Och *et al.* 2013; Feng *et al.* 2014; Jin *et al.* 2016). To trace environmental redox evolution, it is crucial to distinguish redox condition changes of deep seawater from surface seawater and to discern changes in the depth of the marine chemocline. Such information may be retrieved through integrated studies on concentrations of Mo and U and isotopic compositions of S and N in the same sedimentary rock samples.

†Author for correspondence: hfling@nju.edu.cn

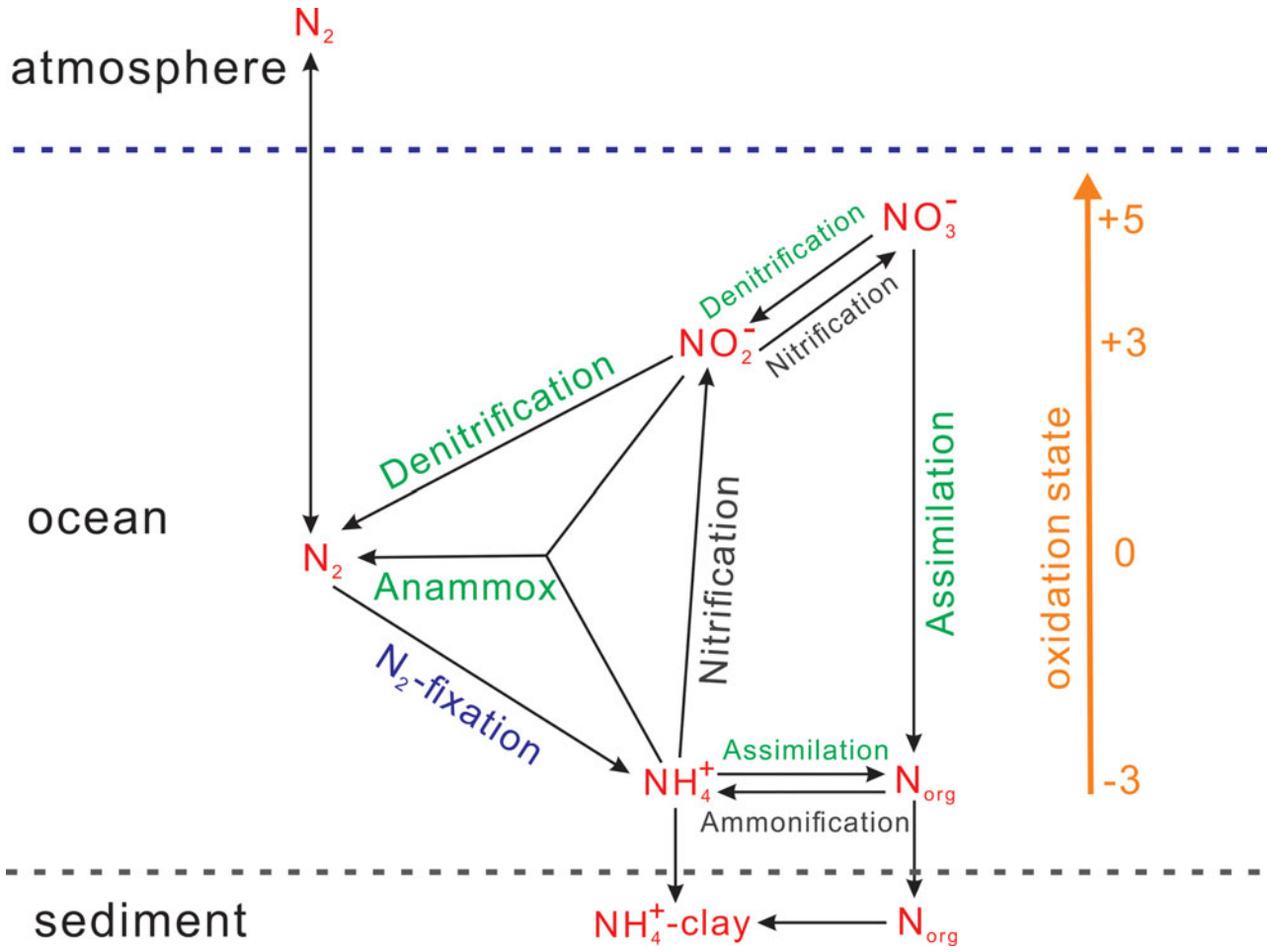

Figure 1. Brief introduction of marine nitrogen cycle, modified from Godfrey & Falkowski (2009).

Systematic and prominent enrichments of redox-sensitive trace-metal elements such as Mo, U and V in sediments deposited in anoxic marine environments with good connections to the open ocean would reflect an increase in the global marine trace-metal element reservoir and a global increase in oxygen at the Earth's surface (Algeo & Lyons, 2006; Scott *et al.* 2008; Sahoo *et al.* 2012), because the global oceanic reservoir of these redox-sensitive elements increased with atmospheric or oceanic oxidation, for example, in the two 'Great Oxidation Events' occurring at *c.* 2.4 Ga and 750–542 Ma (Canfield, 2005; Holland, 2006; Lyons, Reinhard & Planavsky, 2014). However, the local depositional environment to record such enrichments of these elements and such global information must have been anoxic or even sulphidic and connected to the open ocean.

The condition of microbial sulphate reduction (MSR), which results in euxinic seawater and pyrite deposition in high-productivity areas of shelf margins ($SO_4^{2-} + 2CH_2O \rightarrow H_2S + 2HCO_3^-$), can be recorded by sulphur isotopes (Canfield, 2004). The sulphur isotopic composition of sedimentary pyrite formed through MSR is mainly dependent on the isotopic composition of the marine sulphate reservoir (Holser *et al.* 1988) and on the magnitude of MSR isotope fractionation, which varies with sulphate concentration in the seawater (Habicht *et al.* 2002, 2005). MSR processes in pore water within sediments or euxinic seawater under different conditions produce various sulphur isotopes of pyrites in the sediments.

Nitrogen is an essential element for life, and the marine nitrogen cycle is mainly driven by biological processes. There are four main processes for the nitrogen cycle in the modern ocean (as shown in Fig. 1): N_2 fixation by azotobacteria from the atmosphere into organic particulate N; nitrification, in which organic N or NH_4^+ is oxidized to NO_3^-; denitrification, in which NO_3^- is converted back to low-valence nitrogen (N_2O or N_2); and N assimilation, in which NO_3^- or NH_4^+ is assimilated by eukaryotic phytoplankton in the surface seawater (Sigman, Karsh & Casciotti, 2009). These nitrogen cycle processes have different isotope fractionations. Generally, N_2 fixation has small nitrogen isotope fractionations ($\Delta_{PN\text{-}N2} = 0\text{–}2$ ‰) when azotobacteria use molybdenum enzymes (Zerkle *et al.* 2008; Sigman, Karsh & Casciotti, 2009), but a large nitrogen isotope fractionation ($\Delta_{Org\text{-}N2} = -8$ ‰) occurs in N_2 fixation when bacteria only use iron or vanadium enzymes in a sulphidic water column depleted in Mo (Zhang *et al.* 2014). There is no nitrogen isotope fractionation during nitrification when NH_4^+ is transformed to NO_3^- completely under oxic conditions, while the fractionation is large ($\Delta_{NH4+\text{-}NO2-} = \sim 16$ ‰) (Sigman, Karsh &

https://doi.org/10.1017/S0016756817000115 Published online by Cambridge University Press

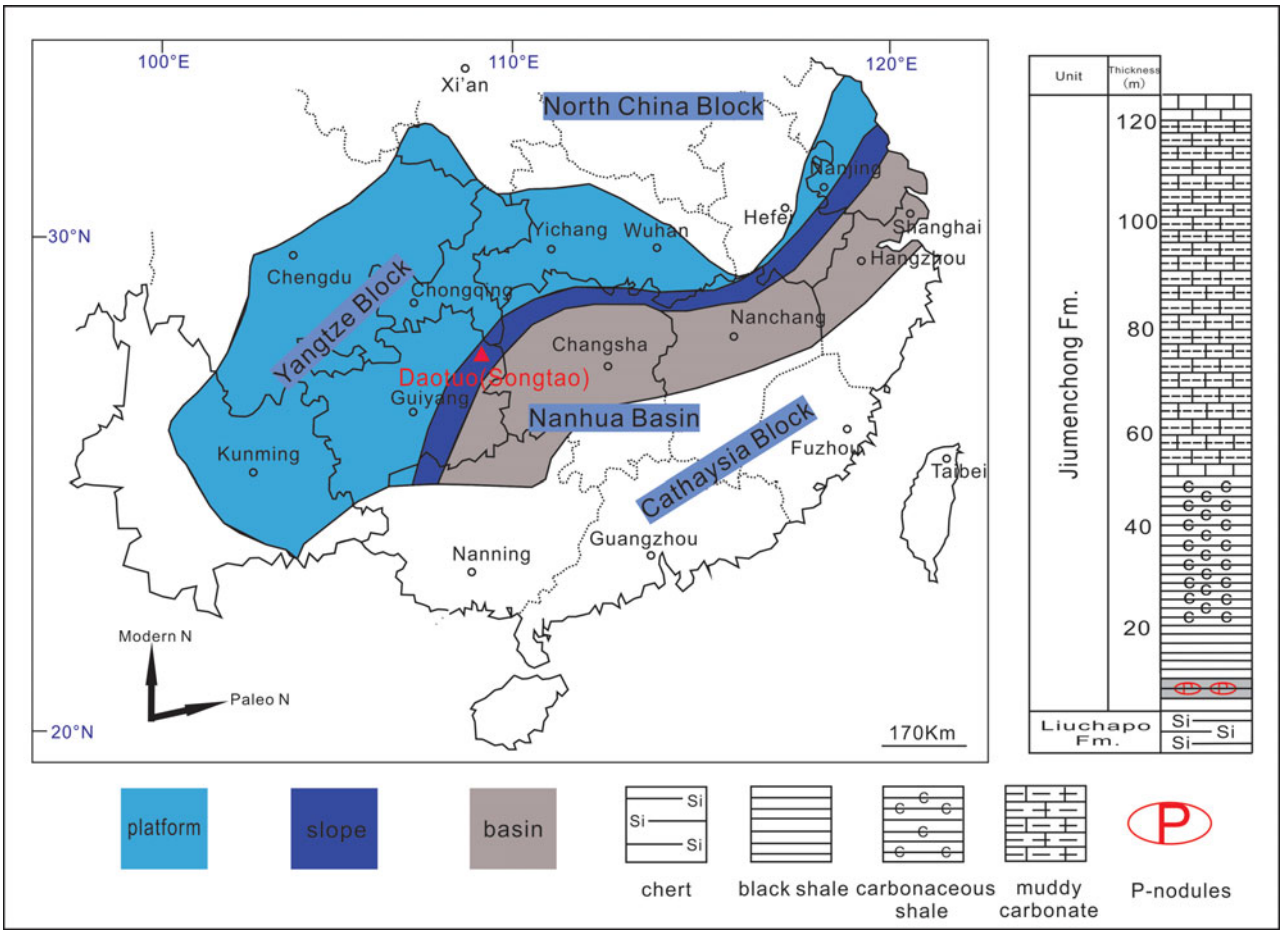

Figure 2. Map of sedimentary facies on the Yangtze block and the stratigraphic column of the drill core at Daotuo (red triangle), Songtao County, NE Guizhou Province, South China, in the transitional period between Ediacaran and early Cambrian, modified from Guo *et al.* (2007).

Casciotti, 2009) when oxygen is not sufficient. A small nitrogen isotope fractionation ($\Delta_{NO3-N2} = 1–4$ ‰) has been found in denitrification occurring in sediments (Prokopenko *et al.* 2006), whereas large fractionations arise in denitrification occurring in the water column ($\Delta_{NO3-N2} = 20–30$ ‰) (Sigman, Karsh & Casciotti, 2009), resulting in a ^{15}N-enriched marine nitrate reservoir. In addition, Higgins *et al.* (2012) proposed a model in which ^{15}N is depleted in eukaryotic biomass when the marine nitrogen reservoir is dominated by NH_4^+ under anoxic conditions because there is a large nitrogen isotope fractionation ($\Delta_{NH4+-Org}$ is up to ~+27 ‰) where primary producers assimilate recycled NH_4^+ as a nitrogen resource. Nitrogen isotopic compositions of organic sediments could record various isotopic signatures of primary producers in the photic zone, reflecting different nitrogen species used by living organisms on continental margins or in basins, thus reflecting redox conditions of surface waters and the depth of the chemocline (Ader *et al.* 2014).

To explore the evolution of the local marine redox environment and biological processes in a typical area on the Yangtze shelf margin during the early Cambrian era, we selected fresh samples from a drill core at Daotuo in Songtao County, northeast Guizhou Province, and measured redox-sensitive element (Mo and U) concentrations, bulk nitrogen isotopes and sulphur isotopes in pyrite in organic-matter-rich black shales and carbonates. Using these data, we aim to trace the variation of marine redox conditions and the nitrogen cycle in this typical area on the Yangtze shelf margin. The results of our analyses probably reflect the local marine information of the Yangtze shelf margin area as spatial heterogeneity of marine redox chemistry may have existed in the Nanhua Basin of South China during the early Cambrian (Jin *et al.* 2016).

2. Stratigraphic setting

In South China, successive marine sedimentary strata of the Nanhua Basin are exposed from the Ediacaran to the Cambrian. Stratum and palaeogeographic reconstruction shows three types of sedimentary facies in the Nanhua Basin: carbonate platform, transitional slope and deep basin (Fig. 2) (Zhu *et al.* 2003, 2007). The studied drill core located at Daotuo in Songtao County of NE Guizhou province, China, represents the mid-depth slope facies of the Nanhua Basin. The rocks of this drill section span from the pre-Cryogenian Banxi Group to the early Cambrian Qingxudong Formation. Our samples collected from the drill core are from the upper Liuchapo Formation (within the

https://doi.org/10.1017/S0016756817000115 Published online by Cambridge University Press

upper part of which the boundary between the Precambrian and Cambrian is located (Chen *et al.* 2015)) to the Jiumenchong Formation (equivalent to the Niutitang Formation, whose middle and upper parts belong to Cambrian Stage 3 (Guo *et al.* 2007)) (see Fig. 2). The Liuchapo Formation consists of dark-grey to black cherts and cherts interbedded with shales and is conformably underlain by the Doushantuo Formation and conformably overlain by the Jiumenchong Formation. The lower Cambrian Jiumenchong Formation is *c.* 120 m thick and consists mainly of carbonaceous shale, black shale and argillaceous carbonate. Near the base of the formation are a black shale layer containing phosphatic nodules and a polymetallic sulphide-rich layer. This formation is overlain by the Palang Formation, which belongs to Cambrian Stage 4. Several ages have been reported for the polymetallic sulphide-rich layer and adjacent black shale, including Pb–Pb isochron ages of 521 ± 54 Ma for the sulphide ores from the Sancha section in Hunan Province, 531 ± 24 Ma for the lower black shales from Zunyi in Guizhou Province (Jiang *et al.* 2006), a Re–Os isochron age of 521 ± 5 Ma for the sulphide ore samples from three sections in Guizhou and Hunan Provinces (Xu *et al.* 2011) and a SHRIMP (sensitive high-resolution ion microprobe) zircon U–Pb age of 522.7 ± 4.9 Ma from a tuffaceous bed in the basal Niutitang Formation in the Taoying section in Guizhou (Wang *et al.* 2012). These ages suggest that the polymetallic sulphide-rich layer should lie at the base of Cambrian Stage 3. Samples for this study from the Daotuo drill core include cherts, black shales, carbonaceous shales and argillaceous carbonates of the early Cambrian upper Liuchapo Formation and Jiumenchong Formation. (Fig. 2).

3. Material and methods

For geochemical and isotopic analyses, samples from the Daotuo drill core of the early Cambrian upper Liuchapo Formation and Jiumenchong Formation were carefully selected to avoid diagenetic or hydrothermal veins. Visible pyrite nodules and veins were discarded to minimize the effect of late diagenetic processes on bulk pyrite chemical analyses. The samples were ground to 200-mesh powder and oven-dried at 60 °C for 3 h in preparation for trace element and isotope analyses. For all samples, we used 2 mol L^{-1} HCl to dissolve carbonate and phosphate, and concentrated $HF + HNO_3$ to fully dissolve the remaining silicate components in Teflon cubes at a temperature of 190 °C. The two solutions of each sample were dried by heating and evaporating, re-dissolved in 3 % HNO_3, and then mixed together for trace element analyses. Trace elements of bulk samples were measured with an ELEMENT II ICP-MS at the State Key Laboratory for Mineral Deposits Research, Nanjing University. Analytical uncertainties for most elements were lower than 5 %.

For analyses of total organic carbon and total nitrogen contents, *c.* 200 mg of bulk powder of each sample was weighed and leached in 2 mol L^{-1} HCl overnight to thoroughly remove carbonate. After centrifugation, the solution was poured out, and the remains were washed and centrifuged with Milli-Q water to remove $CaCl_2$ and residual HCl and then dried at 60 °C. Concentrations of total organic carbon and total nitrogen of the decarbonated samples were measured with a CHN-O-Rapid element analysis instrument at the Center of Modern Analysis, Nanjing University.

For bulk sample N isotopic analyses, 20–30 mg of powder of each sample was weighed in tin capsules according to the total nitrogen content. The powders were combusted to convert total nitrogen to NO_2, and NO_2 was reduced by copper-core pillar into N_2 in the elemental analyser (Flash-EA); the isotopic composition of N_2 was then analysed using a Thermo MAT 253 gas mass spectrometer at the State Key Laboratory for Mineral Deposits Research, Nanjing University. Nitrogen isotopic composition measurements were corrected by laboratory standards Aladdin KNO_3 and urea, with the standard deviation of multiple repeated measurements better than ±0.1 %. Nitrogen isotopic compositions were reported relative to air.

For sulphur isotopic analyses, a wet chemical extraction method was used to leach the pyrite sulphur from each bulk sample. Sulphur in the pyrite was liberated through hot $CrCl_2$, and then reacted with $AgNO_3$ solution to convert it completely into Ag_2S. Approximately 0.4 mg of Ag_2S from pyrite extractions was combusted with ~0.6 mg of V_2O_5 and analysed using a Delta V Advantage isotope ratio mass spectrometer, at the Key Laboratory of Economic Stratigraphy and Palaeogeography, Nanjing Institute of Geology and Palaeontology, Chinese Academy of Science. The NBS-127 ($BaSO_4$), IAEA-S-1 2 3 (Ag_2S) standards and other laboratory standards (FeS_2 and $CuFeS_2$) were used to correct S isotope data, and analytical reproducibility was better than ±0.3 ‰. Sulphur isotope compositions were reported relative to the V-CDT (Vienna Cañon Diablo Troilite) standard.

Major elements of bulk rocks were measured using X-ray fluorescence (XRF) methods in the ALS Laboratory Group's Mineral Division, ALS Chemex, in Guangzhou, China.

4. Results

Concentrations of Al, TOC, TN and trace elements and isotope values of $\delta^{15}N$ and $\delta^{34}S$ for samples of the early Cambrian upper Liuchapo Formation and Jiumenchong Formation are given in Tables 1 and 2. We divide the studied section into three intervals based on the lithology and the variation trends of $\delta^{15}N_{bulk}$ and $\delta^{34}S_{py}$ (Fig. 3). Interval I includes cherts or black cherts in the upper part of the Liuchapo Formation, which probably represents the Fortunian and early Stage 2. Interval II is characterized by phosphatic nodules and a polymetallic enrichment layer in the

https://doi.org/10.1017/S0016756817000115 Published online by Cambridge University Press

Table 1. Al_2O_3, Mo, U and TOC contents of Daotuo drill core samples

Sample	Depth (m)	Lithology	Al_2O_3 (%)	Mo (ppm)	U (ppm)	TOC (%)	Mo/TOC (ppm %$^{-1}$)	U/TOC (ppm %$^{-1}$)
Liuchapo Fm.								
DT-581	0.0	Chert	8.48	8.9	9.5	0.809	10.94	11.70
DT-583	0.7	Black chert	12.25	4.2	7.8	0.240	17.44	32.50
DT-585	1.3	Black chert	6.24	2.9	5.9	2.010	1.44	2.91
DT-587	2.1	Black chert	3.89	1.7	1.5	0.102	16.59	14.62
DT-589	2.7	Black chert	5.15	1.8	3.5	0.156	11.30	22.54
Jiumenchong Fm.								
DT-591	3.4	Black shale	2.86	0.92	8.3	0.288	3.21	28.70
DT-593	3.8	Black shale	7.12	91.5	52.2	4.569	20.02	11.43
DT-595	4.4	Black shale	5.95	20.7	26.0	7.673	2.70	3.39
DT-597	4.9	Black shale	9.45	61.5	78.7	7.222	8.52	10.89
DT-599	5.5	Black shale	13.70	115	50.3	8.098	14.27	6.21
DT-601	6.1	Black shale	13.50	58.7	93.0	5.276	11.12	17.63
DT-603	7.1	Black shale	13.50	50.6	63.2	6.413	7.89	9.85
DT-605	7.7	Black shale	13.90	54.7	52.2	6.917	7.91	7.54
DT-607	8.1	Black shale	13.10	62.6	61.8	5.523	11.33	11.19
DT-609	8.7	Black shale	12.50	56.1	51.4	5.309	10.57	9.67
DT-611	9.3	Black shale	11.75	63.4	49.5	4.649	13.64	10.65
DT-613	9.9	Black shale	12.65	51.6	39.7	3.984	12.96	9.96
DT-615	11.2	Black shale	12.80	38.8	33.1	3.842	10.10	8.61
DT-a62	15.2	Black shale	11.45	43.3	26.5	3.276	13.21	8.08
DT-a64	17.2	Black shale	13.45	56.6	38.0	3.106	18.23	12.23
DT-a66	19.2	Black shale	13.80	42.9	28.0	3.020	14.21	9.28
DT-a68	21.2	Carbonaceous shale	13.85	8.1	15.2	4.016	2.02	3.79
DT-a70	23.2	Carbonaceous shale	13.75	12.9	19.5	4.948	2.61	3.94
DT-1004	25.7	Carbonaceous shale	13.45	4.5	7.0	0.625	7.20	11.27
DT-1010	31.7	Carbonaceous shale	17.70	0.91	4.4	0.333	2.75	13.11
DT-1013	34.0	Carbonaceous shale	15.95	1.3	5.0	0.973	1.31	5.18
DT-1016	36.5	Carbonaceous shale	16.30	0.9	4.1	0.401	2.27	10.26
DT-1022	42.0	Carbonaceous shale	12.45	5.0	10.8	3.618	1.39	2.97
DT-1025	44.8	Carbonaceous shale	8.88	9.0	16.4			
DT-1028	47.8	Carbonaceous shale	8.08	1.9	3.5	0.786	2.42	4.50
DT-1031	50.1	Muddy limestone	3.02	5.5	11.0	0.979	5.62	11.23
DT-1037	58.7	Muddy limestone	0.64	1.3	5.6	0.360	3.67	15.43
DT-1043	65.0	Muddy limestone	3.80	4.9	7.6			
DT-1046	67.5	Muddy limestone	0.94	1.2	2.8			
DT-1049	69.0	Carbonaceous shale	13.50	2.5	5.7	2.803	0.88	2.04
DT-1056	76.0	Carbonaceous shale	17.25	2.9	9.6			
DT-1059	78.0	Muddy limestone	18.30	4.5	7.0	1.226	3.70	5.72
DT-1062	80.5	Muddy limestone	18.65	5.3	6.4	0.592	8.87	10.82
DT-1065	83.5	Muddy limestone	18.40	20.3	15.4	1.453	13.94	10.60
DT-1068	86.5	Muddy limestone	16.90	24.1	17.7	0.955	25.24	18.52
DT-1071	89.0	Muddy limestone	17.70	13.8	13.3	0.248	55.37	53.41
DT-1074	92.0	Muddy limestone	18.40	13.1	11.3	1.558	8.41	7.28
DT-1077	94.5	Muddy limestone	18.45	9.7	9.4	1.247	7.75	7.51
DT-1080	97.5	Muddy limestone	13.00	6.9	7.2	0.793	8.75	9.08
DT-1083	99.5	Muddy limestone	6.37	2.9	3.4	0.599	4.87	5.75
DT-1084	100.5	Muddy limestone	12.45	4.4	6.6	0.204	21.78	32.49
DT-1085	102.8	Muddy limestone	6.19	2.9	3.0	0.428	6.80	7.01
DT-1091	108.8	Muddy limestone	9.14	3.6	5.2	0.308	11.77	17.01
DT-1097	111.6	Muddy limestone	3.02	1.7	2.3	0.100	16.93	22.55
DT-1100	114.1	Muddy limestone	5.03	5.0	5.3	0.239	20.85	22.14
DT-1103	116.6	Limestone	10.85	4.7	5.2	0.368	12.64	14.22
DT-1106	119.6	Limestone	14.10	0.54	3.2	0.404	1.33	7.91
DT-1109	122.1	Limestone	12.10	5.0	6.5	0.508	9.78	12.76

lower Jiumenchong Formation black shales, which represents the upper Stage 2 and early Stage 3 because the polymetallic sulphide-rich layer occurs just below the boundary between Stages 2 and 3 (Jiang *et al.* 2006; Xu *et al.* 2011). Interval III consists of carbonaceous shales and muddy limestones of the middle and upper Jiumenchong Formation, possibly representing the middle and upper Stage 3.

The studied samples from Interval I have low concentrations of Mo (0.92–8.9 ppm) and U (1.5–9.5 ppm). The $\delta^{34}S_{py}$ values of this interval are relatively high (5.1–15.9 ‰, averaging 9.4 ‰). All studied samples from Interval I have relatively low $\delta^{15}N_{bulk}$ values (1.2–1.9 ‰), except for one sample that has a high value of 3.5 ‰ occurring as a sharp positive excursion.

The Interval II black shale samples have high concentrations of Mo and U (averages of 57.9 and 49.6 ppm, respectively), with one black shale sample from the polymetallic sulphide-rich layer (Guo *et al.* 2007; Xu *et al.* 2012; Och *et al.* 2013) showing the highest concentrations of Mo (115 ppm) and U (93.0 ppm) in all analysed samples of the section. In Interval II the lowest $\delta^{34}S_{py}$ values (−16.8 to −14.8 ‰)

https://doi.org/10.1017/S0016756817000115 Published online by Cambridge University Press

Table 2. TOC, TN, Sulphur- and nitrogen-isotope ratios of Daotuo drill core samples

Sample	Depth (m)	Lithology	$\delta^{34}S$ (‰)	$\delta^{15}N$ (‰)	TOC_{decarb} (%)	TN_{decarb} (%)	$(C/N)_{decarb}$ molar ratios
Liuchapo Fm.							
DT-581	0.0	Chert	15.9	1.0	1.286	0.104	14.426
DT-583	0.7	Black chert		3.5	0.262	0.071	4.305
DT-585	1.3	Black chert	3.2	1.9	2.388	0.068	40.971
DT-587	2.1	Black chert	5.1	0.4	0.187	0.042	5.194
DT-589	2.7	Black chert		0.2	0.284	0.055	6.025
Jiumenchong Fm.							
DT-591	3.4	Black shale	13.2	-1.2	1.067	0.097	12.833
DT-593	3.8	Black shale	-8.6	-2.4	5.677	0.132	50.176
DT-595	4.4	Black shale	5.1	-1.0	11.907	0.199	69.806
DT-597	4.9	Black shale	-16.8	-1.1	9.655	0.219	51.435
DT-599	5.5	Black shale	-14.8	-3.2	8.572	0.196	51.024
DT-601	6.1	Black shale		1.0	5.849	0.143	47.719
DT-603	7.1	Black shale		0.9	6.809	0.144	55.166
DT-605	7.7	Black shale	0.03	1.2	7.299	0.192	44.352
DT-607	8.1	Black shale		1.3	5.891	0.176	39.051
DT-609	8.7	Black shale	3.9	1.5	5.709	0.167	39.884
DT-611	9.3	Black shale		1.6	5.018	0.158	37.052
DT-613	9.9	Black shale	2.0	1.7	4.210	0.148	33.187
DT-615	11.2	Black shale	5.6	1.4	4.108	0.157	30.527
DT-a62	15.2	Black shale	3.6	1.5	3.594	0.138	30.384
DT-a64	17.2	Black shale	4.1	1.5	3.331	0.155	25.072
DT-a66	19.2	Black shale	1.5	1.4	3.325	0.159	24.397
DT-a68	21.2	Carbonaceous shale	1.4	1.0	4.317	0.155	32.494
DT-a70	23.2	Carbonaceous shale		1.0	5.679	0.176	37.645
DT-1004	25.7	Carbonaceous shale	4.7	1.2	0.864	0.154	6.545
DT-1010	31.7	Carbonaceous shale	-2.9	0.9	0.387	0.172	2.625
DT-1013	34.0	Carbonaceous shale	10.2	0.8	0.388	0.201	2.252
DT-1016	36.5	Carbonaceous shale	19.2	0.8	1.191	0.190	7.313
DT-1022	42.0	Carbonaceous shale		0.8	0.499	0.189	3.080
DT-1025	44.8	Carbonaceous shale	7.6	0.5	4.724	0.185	29.791
DT-1028	47.8	Carbonaceous shale		0.5	1.608	0.198	9.475
DT-1031	50.1	Muddy limestone	-0.9	0.2	4.826	0.222	25.362
DT-1037	58.7	Muddy limestone	8.9	0.2	6.421	0.150	49.942
DT-1043	65.0	Muddy limestone	5.9	− 0.4	3.182	0.136	27.297
DT-1046	67.5	Muddy limestone		0.3	2.491	0.168	17.298
DT-1049	69.0	Carbonaceous shale	1.8	− 0.6	2.294	0.159	16.833
DT-1056	76.0	Carbonaceous shale	4.9	− 1.1	1.314	0.168	9.125
DT-1059	78.0	Muddy limestone		− 0.7	0.636	0.159	4.667
DT-1062	80.5	Muddy limestone	4.6	− 1.1	1.590	0.170	10.912
DT-1065	83.5	Muddy limestone		− 0.9	1.013	0.161	7.341
DT-1068	86.5	Muddy limestone	19.2	− 1.0	0.274	0.039	8.197
DT-1071	89.0	Muddy limestone		− 1.2	1.703	0.151	13.158
DT-1074	92.0	Muddy limestone	18.0	− 1.7	1.338	0.152	10.270
DT-1077	94.5	Muddy limestone		− 1.4	0.870	0.157	6.465
DT-1080	97.5	Muddy limestone	13.5	− 0.9	0.679	0.094	8.427
DT-1083	99.5	Muddy limestone		− 0.7	0.217	0.036	7.033
DT-1084	100.5	Muddy limestone		− 0.9	0.492	0.087	6.598
DT-1085	102.8	Muddy limestone	8.1	− 0.8	0.357	0.060	6.942
DT-1091	108.8	Muddy limestone	10.2	− 1.0	0.889	0.124	8.364
DT-1097	111.6	Muddy limestone	1.8	− 0.8	0.157	0.015	12.212
DT-1100	114.1	Muddy limestone		− 0.5	0.300	0.032	10.938
DT-1103	116.6	Limestone	13.1	− 1.1	0.387	0.066	6.841
DT-1106	119.6	Limestone	11.1	− 1.1	0.445	0.084	6.181
DT-1109	122.1	Limestone	8.5	− 1.0	0.564	0.077	8.546

of all the studied samples also occur. In addition, the mean $\delta^{34}S_{py}$ of Interval II is relatively low (−1.3 ‰). At the top of Interval II, the $\delta^{34}S_{py}$ values rise and become positive (from 0.03 ‰ to 5.6 ‰). The $\delta^{15}N_{bulk}$ values in Interval II are very low, from −1.0 ‰ to −3.2 ‰, but rise to positive values (0.9–1.7 ‰) at the top of this interval.

In Interval III, there are relatively low concentrations of Mo (<25 ppm) and of U (<18 ppm) except for two samples (20.3 and 24.1 ppm). The $\delta^{34}S_{py}$ values of most samples from this interval are high (1.4–19.2 ‰, averaging 8.0 ‰) except for two negative values close to 0 ‰. The $\delta^{15}N_{bulk}$ values are between 2 ‰ and −2 ‰ with a decreasing trend from the bottom to the top of this interval.

5. Discussion

5.a. Marine environment in the Yangtze shelf margin area implied by covariations of Mo vs U and Mo vs TOC

Trace elements in black shale can reflect information about the lithogenous sources from the weathering and erosion of the continents or the authigenic seawater

https://doi.org/10.1017/S0016756817000115 Published online by Cambridge University Press

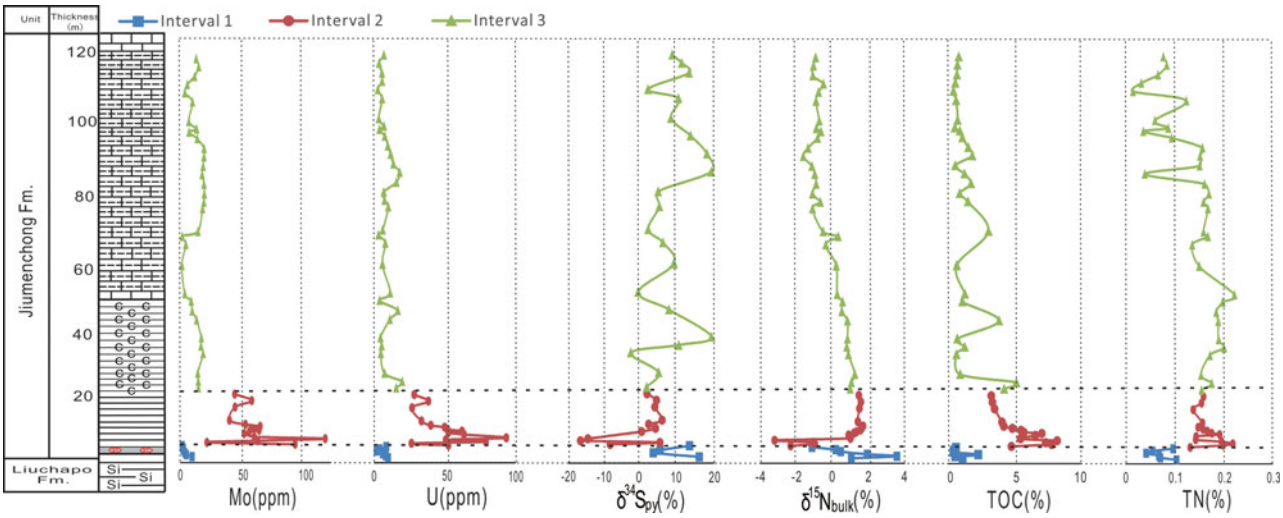

Figure 3. Concentrations of Mo, U, C and N_{decarb}, and isotope compositions of sulphur and nitrogen, in early Cambrian samples from Daotuo drill core.

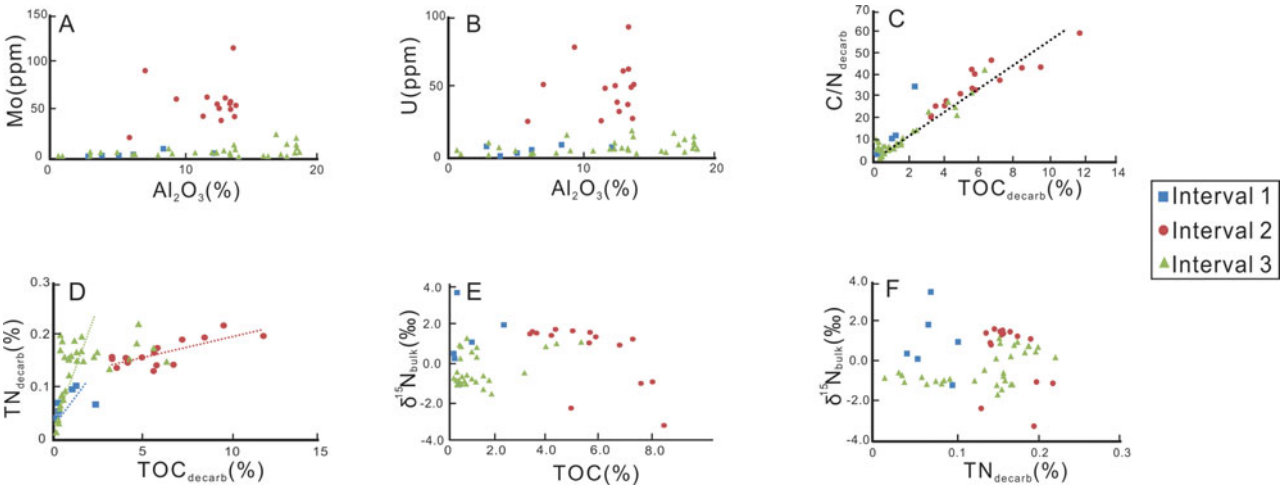

Figure 4. Analyses of Mo, U concentrations vs Al_2O_3, total nitrogen (TN_{decarb}), total organic carbon (TOC_{decarb}) and C/N_{decarb} data in the decarbonated samples of Daotuo drill core.

source (Goldberg, 1963; Piper & Calvert, 2009). Authigenic seawater components, such as organic matter, pyrite and phosphorite, can record the original environmental information of the ocean. Because Al is an essential element of aluminosilicate rocks in weathering and eroding continents and its concentrations in detritus eroded from continents are similar, and much higher than that in seawater, the content of Al_2O_3 is frequently used to evaluate the fraction of trace elements from terrigenous debris in a marine deposit (Taylor & McLennan, 1985; Wedepohl, 1995; Piper & Calvert, 2009). As shown in Figure 4A and B, there is no clear correlation between Mo or U concentrations and Al_2O_3 concentrations in the studied samples. Compared with the low Mo and U concentrations in PAAS (Post-Archaean Australian Shale, Mo = 1 ppm, U = 3.1 ppm; Taylor & McLennan, 1985), which represents fine detrital sediments with little or no organic matter, Mo and U concentrations in most of the studied samples are clearly higher. These observations indicate that Mo and U contained in most of the studied samples were dominantly deposited from a seawater source and thus could record information about the marine environment.

According to studies on modern marine sediments, Mo concentrations in sediments can be up to or greater than 100 ppm under a continuous euxinic marine environment, while they are lower than 25 ppm under oxic or dysoxic environmental conditions (Scott & Lyons, 2012). Strong microbial sulphate reduction in high-productivity marine settings such as semi-restricted shelf margins creates a euxinic marine environment (with the presence of S^{2-} in seawater) and stimulates the precipitation of Mo (Canfield, 2004; Li *et al.* 2010). Unlike the precipitation of Mo, which requires sulphidic redox conditions, soluble U (VI) from oxic seawater can be reduced to insoluble U (IV) and deposited into sediments under anoxic conditions without sulphide (Tribovillard *et al.* 2006). Based on analyses of iMo and U concentrations of sediments from various representative modern marine environments, different covariations of enrichment factors of

https://doi.org/10.1017/S0016756817000115 Published online by Cambridge University Press

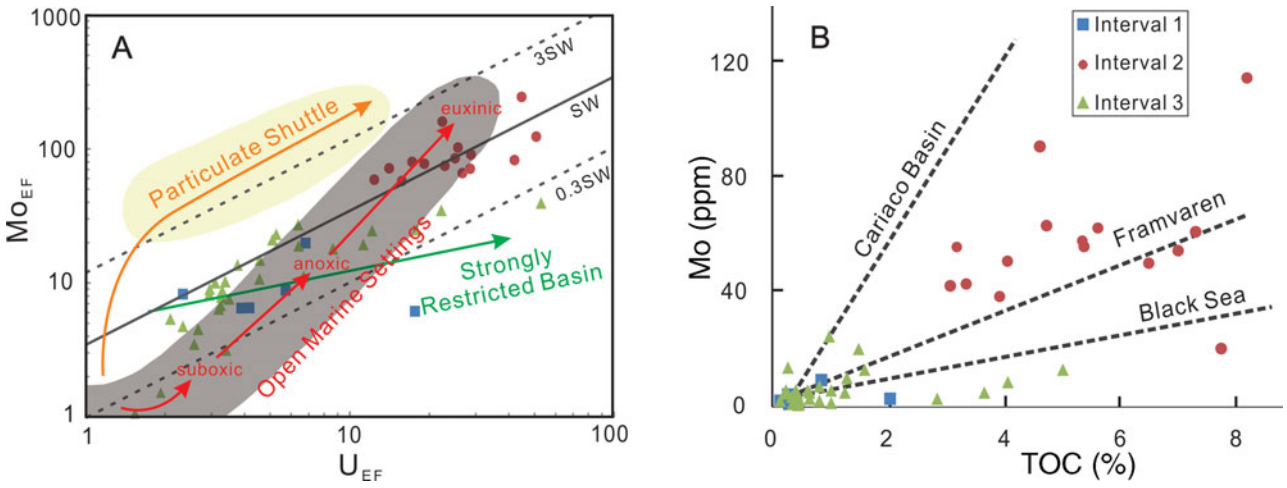

Figure 5. (A) Mo$_{EF}$ vs U$_{EF}$ covariation and (B) Mo vs TOC covariation patterns of Daotuo drill core samples. SW: modern seawater. Modified from Algeo & Tribovillard (2009) and Algeo & Lyons (2006), respectively.

Mo and U (expressed as Mo-$_{EF}$ and U-$_{EF}$, respectively, and defined by X-$_{EF}$ = (X/Al)$_{sample}$/(X/Al)$_{PAAS}$; Taylor & McLennan, 1985) in sediments have been found and used to distinguish various redox environments (Algeo & Tribovillard, 2009; Tribovillard *et al.* 2012). Algeo & Tribovillard (2009) show that different Mo$_{EF}$ vs U$_{EF}$ covariation patterns reflect various redox conditions and particulate shuttles of marine sedimentary environments, based on a study of three different modern low-oxygen marine environments (the California Borderlands as an open marine setting, Cariaco Basin, Venezuela, as a particulate shuttle basin, and the Black Sea as a strongly restricted basin).

Rapid Mo precipitation in a strongly restricted euxinic basin would deplete dissolved Mo in the water column in the basin due to limited Mo replenishment from the open ocean. Therefore, Mo/TOC ratios of sediments would decrease with the enhancement of the extent of water-mass restriction. Research on modern marine sedimentary environments with diverse extents of restriction (Black Sea; Framvaren Fjord, Norway; Cariaco Basin; and Saanich Inlet, Canada) has found various slopes of the Mo–TOC linear covariation, which can be used to constrain the extents of marine water-mass restriction of palaeoenvironments (Algeo & Lyons, 2006; Algeo & Rowe, 2012).

In this study, we apply Mo-$_{EF}$ vs U-$_{EF}$ and Mo vs TOC covariations to the Daotuo drill core samples to constrain the evolution of redox conditions and the restriction extents of the sedimentary environment in the study area of the Yangtze shelf margin during the early Cambrian. Mo$_{EF}$–U$_{EF}$ covariation of the Daotuo drill core samples is shown in Figure 5A. The overall distribution of the studied samples shows a well-defined pattern of Mo$_{EF}$–U$_{EF}$ covariation, which slightly deviates from the pattern defined for unrestricted modern marine settings (grey area in Figure 5A; Algeo & Tribovillard, 2009). This likely indicates a weakly restricted environment on the Yangtze shelf margin, without particulate shuttle enrichment for Mo, which is consistent with the implication of the Mo/TOC data of the samples discussed below. Furthermore, the oceanic Mo concentration in the early Cambrian is estimated as 50 nmol L^{-1} (X. Wang *et al.* 2015), approximately half of that in the modern ocean (102 nmol L^{-1}), implying that the oceanic Mo reservoir was higher than in earlier times (e.g. 10–20 nmol L^{-1} in the Mesoproterozoic) (Scott *et al.* 2008). Aqueous Mo in the Nanhua Basin, though precipitating in deep euxinic water, was replenished from the open ocean whose Mo reservoir was evidently increased compared with that of the Mesoproterozoic. Because U precipitates at the Fe (II) – Fe (III) boundary (i.e. anoxic–suboxic boundary) while Mo precipitates in sulphidic water or sediments, the low Mo-$_{EF}$ (from 0.7 to 38) and low Mo/U weight ratios (from 0.1 to 1.4, which are much lower than the modern seawater value of 3.1) of the samples from Intervals I and III reflect suboxic or anoxic marine conditions in the Cambrian Fortunian Stage to lower Stage 2 and in upper Stage 3. In contrast, Interval II has significantly high Mo-$_{EF}$ (from 57.3 to 242) and Mo/U weight values (up to 2.3), suggesting that the marine environment was briefly in euxinic conditions from upper Stage 2 to lower Stage 3.

Mo–TOC covariation patterns of the studied samples from the three intervals are shown in Figure 5B. The Mo/TOC ratios of the Black Sea (a strong restricted basin), Framvaren Fjord and Cariaco Basin (an Fe–Mn particulate shuttle area) are 4.5 ± 1, 9 ± 2 and 25 ± 5, respectively (Algeo & Lyons, 2006). The Mo/TOC values of Interval I samples range from 1.44 to 16.6 ppm %$^{-1}$ (averaging 10.2 ppm %$^{-1}$), those of Interval II from 2.7 to 20.0 ppm %$^{-1}$ (averaging 11.8 ppm %$^{-1}$), and those of Interval III from 0.88 to 50.4 ppm %$^{-1}$ (averaging 9.68 ppm %$^{-1}$). Cross-plots of Mo content with TOC content of Interval I and II samples are distributed in the area between the covariation lines of Cariaco Basin and Framvaren Fjord sediments, indicating a weakly restricted marine environment during deposition of

https://doi.org/10.1017/S0016756817000115 Published online by Cambridge University Press

the two intervals. In this figure, a few samples of Interval III are plotted in the area below the Black Sea line, suggesting a more restricted environment in this period than in the previous two intervals. In general, the mean Mo/TOC value of the studied samples is *c.* 10 ppm $\%^{-1}$, much higher than that of the Black Sea (4.5 ± 1 ppm $\%^{-1}$), suggesting a weakly restricted sedimentary environment on the Yangtze shelf margin area in the early Cambrian era.

5.b. Marine sulphate concentration of the Yangtze margin area during the early Cambrian

Several factors control the sulphur isotopic compositions of pyrites precipitating from anoxic seawater into black shales or other reduced sediments. One factor is the sulphate concentration in the seawater, which mainly controls the MSR fractionation in seawaters. Laboratory experiments demonstrate that fractionation caused by MSR decreases with falling sulphate concentration when sulphate concentration in seawater is lower than 2 mmol L^{-1} (Harrison & Thode, 1958; Canfield, 2001; Habicht *et al.* 2005) and that the MSR fractionation is large when sulphate concentration in the seawater is ample (much higher than 2 mmol L^{-1}). The ocean sulphate concentration effectively reflects the oxygen level of the Earth's surface because the primary source of sulphate in seawater is the oxidative weathering of pyrite on the continents (Canfield, 2004) and because a greater total of anoxic bottom water areas in the ocean provides more opportunities to sequester sulphate in the seawater through MSR. The other factor controlling sulphur isotopic compositions of pyrites precipitating in sediments is the isotopic composition of the oceanic sulphate reservoir, which depends on the isotopic composition of sulphur input and output (Strauss, 1999). In a relatively restricted marine environment, the two different sulphate origins, i.e. the riverine sulphate and the oceanic sulphate reservoirs, may result in diverse isotopic compositions of local seawater sulphate in various nearshore areas and thus may generate variable pyrite sulphur isotopic compositions in different sedimentary environments (Feng *et al.* 2014). Riverine sulphate generally has a low S-isotope composition (~+8 ‰) (Berner & Berner, 1996). The large variation range and relatively strong fluctuation of the $\delta^{34}S_{py}$ values of the samples in this study (from −16.8 ‰ to 19.2 ‰) cannot be explained by simple sulphate source exchange. Other factors, such as the oxidative portion of the microbial sulphur cycle and sulphur disproportionation, can result in a substantial increase in sulphur fractionation relative to primary MSR, while these two processes require a relatively oxic condition (Jones & Fike, 2013). In our study area, an anoxic–euxinic marine redox condition and a weakly restricted environment are supported by trace element proxies (Mo_{EF}, U_{EF} covariation and Mo–TOC covariation). These data suggest that marine sulphate concentration was the most important factor for sulphur fractionation during MSR for the samples in this study.

Based on the empirical relationship between seawater sulphate concentrations and $\Delta^{34}S_{CAS\text{-}PY}$ analysed for 81 modern depositional systems, Algeo *et al.* (2015) proposed an MSR-trend method to quantitatively estimate the mean global seawater SO_4^{2-} concentration in a specific geological period: $\log[SO_4^{2-}] = (\log(\Delta^{34}S_{CAS\text{-}PY}) - 1.10)/0.42$. The upper and lower uncertainty limits for estimates of marine $[SO_4^{2-}]$ based on this relationship are $\log[SO_4^{2-}] = (\log(\Delta^{34}S_{CAS\text{-}PY}) - 1.18)/0.40$ and $\log[SO_4^{2-}] = (\log(\Delta^{34}S_{CAS\text{-}PY}) - 1.02)/0.44$, respectively (Algeo *et al.* 2015). The $\delta^{34}S$ values of the global seawater sulphate during the terminal Neoproterozoic to the early Cambrian were estimated between 25 ‰ and 35 ‰ (Strauss, 1997; Shen *et al.* 1998; Goldberg, Poulton & Strauss, 2005). Based on these estimated seawater sulphate $\delta^{34}S$ values, our $\delta^{34}S$ results for pyrite and the MSR-trend method, we calculated the seawater sulphate concentrations in the three intervals (Table 3). Because of the uncertainties in $\Delta^{34}S_{CAS\text{-}PY}$ and S-isotope fractionation associated with MSR, minimum $\Delta^{34}S_{CAS\text{-}PY}$ values with the upper uncertainty limit equation are used to estimate minimum marine $[SO_4^{2-}]$, and maximum $\Delta^{34}S_{CAS\text{-}PY}$ values with the lower uncertainty limit equation are used to estimate maximum marine $[SO_4^{2-}]$. Assuming that pyrite formed in sediment pore water during early diagenesis would yield higher $\delta^{34}S_{py}$ than pyrite formed in seawater, as depletion of SO_4^{2-} occurring in the pore water would cause a decrease in fractionation between SO_4^{2-} and S^{2-} during MSR. Thus, the calculated $\Delta^{34}S_{CAS\text{-}PY}$ values are likely minimum values if part of the pyrites was formed by MSR occurring in the sediments (e.g. Interval III), and the resulting seawater sulphate estimates are minimum values. Because, in periods of euxinic marine environments, pyrites were formed largely in sulphidic seawater, and, in periods of non-euxinic environments, pyrites were mainly formed in sediments, only $\delta^{34}S$ values of pyrites in euxinic black shales could reflect seawater sulphate concentrations. However, seawater sulphate concentrations could be higher than calculated seawater sulphate concentrations calculated from $\delta^{34}S$ values of pyrites in non-euxinic sedimentary rocks.

Estimates of marine sulphate concentration are shown in Table 3; the studied samples from Interval I (cherts from the Liuchapo Formation) of the Daotuo drill core have relatively high $\delta^{34}S_{py}$ (up to 15.9 ‰; mean value of 9.4 ‰), indicating relatively low oceanic sulphate concentration (*c.* 1.7–5.4 mmol L^{-1}; the lowest value is 0.3 mmol L^{-1}) and MSR in sediment pore water with anoxic bottom water in the Cambrian Fortunian and lower Stage 2 (Fig. 6A). Black shales in Interval II of the lower Jiumenchong Formation show evidently low $\delta^{34}S_{py}$ (down to −16.8 ‰; mean value of −1.3 ‰) and high Mo concentrations (up to 115.6 ppm), indicating relatively high marine sulphate concentration (mainly *c.* 5.8–12.4 mmol L^{-1} with the

https://doi.org/10.1017/S0016756817000115 Published online by Cambridge University Press

Table 3. Approximate estimated marine sulphate concentrations on the Yangtze shelf margin in the early Cambrian with the MSR-trend method

		$\delta^{34}S_{CAS}$ (‰)	$\delta^{34}S_{py}$ (‰)	$\Delta^{34}S_{CAS\text{-}PY}$ (‰)	$[SO_4^{2-}]$ mean (mmol/L)	$[SO_4^{2-}]$ upper limit (mmol/L)	$[SO_4^{2-}]$ lower limit (mmol/L)
Interval I	mean	35	9.4	25.6	5.4	3.7	7.6
		25	9.4	15.6	1.7	1.1	2.5
	min.	35	15.9	19.1	2.7	1.8	3.9
		25	15.9	9.1	0.5	0.3	0.7
Interval II	mean	35	− 1.3	36.3	12.5	8.9	16.9
		25	− 1.3	26.3	5.8	4.0	8.1
	max.	35	− 16.8	51.8	29.0	21.7	37.8
		25	− 16.8	41.8	17.4	12.7	23.2
Interval III	mean	35	8.0	27.0	6.1	4.2	8.6
		25	8.0	17.0	2.0	1.3	3.0
	min.	35	19.2	15.8	1.7	1.1	2.5
		25	19.2	5.8	0.2	0.1	0.3

highest up to 37.8 mmol L^{-1}). Strong MSR occurred in the seawater, probably due to the increased riverine sulphate input and a pulse of shrinking total area of anoxic bottom waters in global oceans (Chen *et al.* 2015). A large quantity of Mo, U and other redox-sensitive metallic elements also precipitated in this euxinic seawater environment, forming the euxinic black shale bearing the polymetallic enrichment layer (Fig. 6B). The sulphur isotopes in Interval III returned to relatively heavy except for two samples and then fluctuated with time in this period (mean $\delta^{34}S_{py}$ is 8.0 ‰). Such isotopic variation may reflect variable sulphate concentration in the seawater and relatively low average concentration of marine sulphate (2.0–6.1 mmol L^{-1}; the lowest value is 0.1 mmol L^{-1}), if the sulphur isotopic compositions of the seawater sulphate reservoir remained nearly unchanged from slope to basin in the Nanhua Basin during this short period (Feng *et al.* 2014). The deep marine environment became anoxic again without significant Mo precipitation, and MSR mainly occurred within the sediments (Fig. 6C). It should be noted that pyrites are mainly formed in sediments in Intervals I and III, and the estimates of marine sulphate concentrations in these periods are probably lower than the actual values. Only the estimates derived from the pyrites formed in sulphidic seawater in Interval II could reflect the actual marine sulphate concentrations.

5.c. Marine nitrogen cycle of the Yangtze margin area during the early Cambrian

Early diagenesis and thermal maturation during burial of organic matter may affect nitrogen isotopic compositions of bulk samples. To evaluate whether the nitrogen isotopic values reflect the primary marine information or not, we examined the relationships between total organic carbon (TOC_{decarb}), total nitrogen (TN_{decarb}), C/N_{decarb} molar ratios and $\delta^{15}N$ values in the decarbonated samples (Fig. 4C, D, E, F). The relatively clear linear correlation between TN_{decarb} and TOC_{decarb} (Fig. 4D) indicates that the nitrogen in the sediments is derived from two components, an organic component from primary production and an inorganic clay-bound nitrogen component originating from digestion of organic matter by microorganisms, represented by the intercept on the TN axis (Calvert, 2004; D. Wang *et al.* 2015). The mean C/N molar ratio in modern marine sediments is *c.* 6 (Redfield, 1963), while Precambrian samples often have much higher C/N molar ratios (>100) due to the loss of N during diagenesis through degradation of organic matter via microorganisms (e.g. D. Wang *et al.* 2015; Wei *et al.* 2016). The studied samples have an average C/N molar ratio of 21.3 and show a clear linear correlation between C/N and TOC_{decarb} (Fig. 4C), suggesting weak loss of organic nitrogen from the studied samples during their early diagenesis (Cremonese *et al.* 2013). The $\delta^{15}N_{bulk}$ values of sediments normally increase as organic matter degrades, usually with preferential loss of ^{14}N during diagenesis (Pinti *et al.* 2007; Thomazo, Ader & Philippot, 2011). There is no obvious linear correlation between $\delta^{15}N_{bulk}$ and TOC or TN_{decarb} (Fig. 4E, F), suggesting that the nitrogen isotopes of the studied samples have not changed significantly with the nitrogen loss of the organic matter. In summary, the nitrogen isotopic data of the studied samples principally record the primary marine geochemical information of the Yangtze shelf margin.

Based on nitrogen isotopic compositions of the studied bulk samples from the Daotuo drill core, combined with trace elements of the bulk samples and sulphur isotopes in pyrites, we discuss the nitrogen cycles for the early Cambrian Yangtze shelf margin as follows.

5.c.1. Cambrian Fortunian and lower Stage 2 (Interval I)

In the stratified redox ocean, ^{15}N-enriched NO_3^- would occur in the oxic or dysoxic surface seawater, while ^{15}N-depleted NH_4^+ would occur in the anoxic deep seawater (Higgins *et al.* 2012; Ader *et al.* 2014). For the Cambrian Fortunian and lower Stage 2 (Interval I), the low Mo concentrations and relatively high $\delta^{34}S_{py}$ values of this study and Fe speciation data available from the literature (Och *et al.* 2013; Feng *et al.* 2014; Chen *et al.* 2015) indicate that the Nanhua

https://doi.org/10.1017/S0016756817000115 Published online by Cambridge University Press

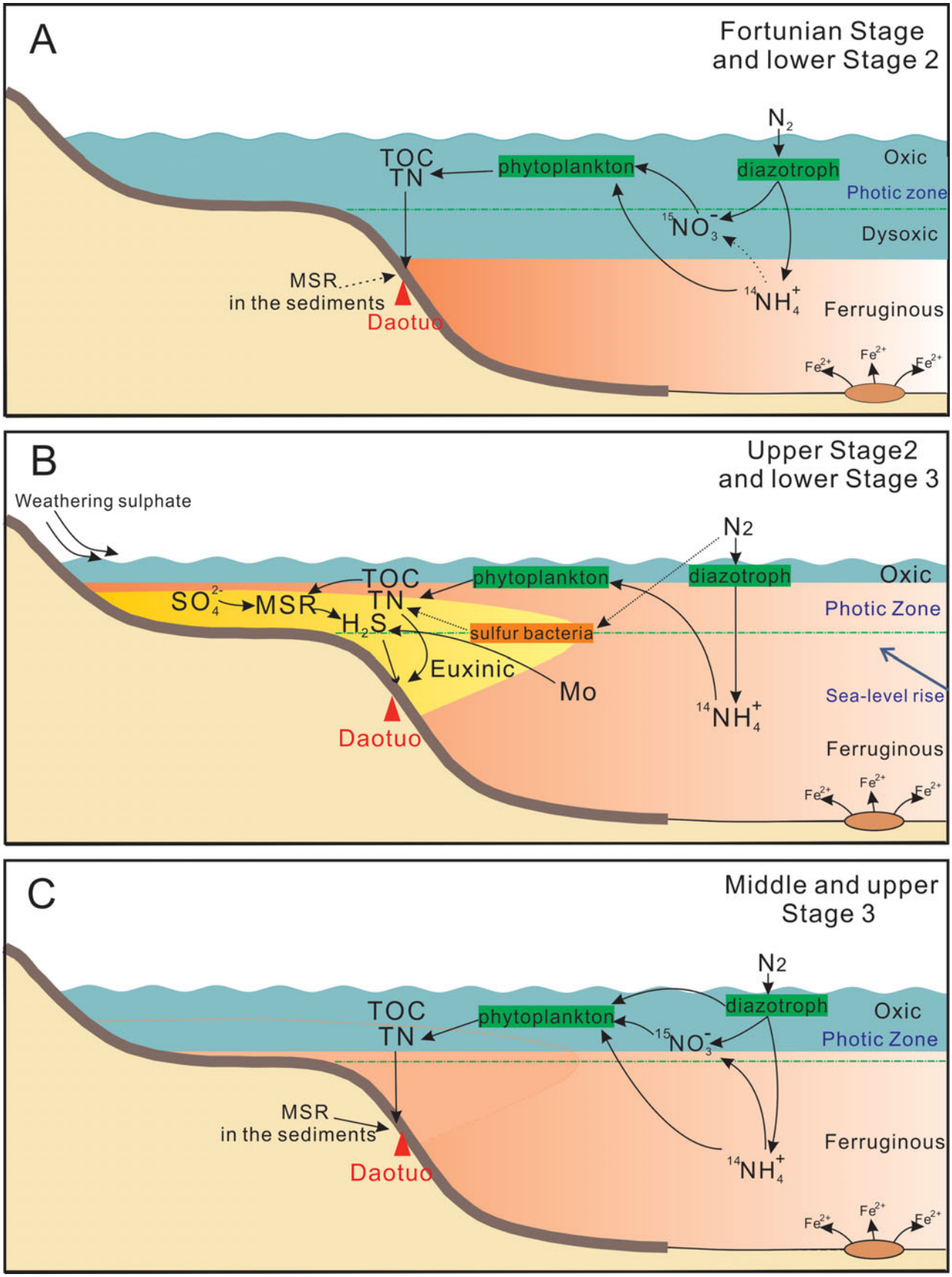

Figure 6. Schematic scenarios for geochemistry cycle in the early Cambrian ocean on the Yangtze shelf margin with three intervals: (A) Cambrian Fortunian and lower Stage 2, the relatively deep chemocline which separates anoxic deep water from oxic surface water and the oxic photic zone. (B) Upper Stage 2 and lower Stage 3, the rise of the chemocline and the expansion of the mid-depth sulphidic zone on the Yangtze margin (based on Li *et al.* (2015)) with the anoxic, or even euxinic, photic zone through upwelling deep water. (C) Middle and upper Stage 3, the depression of the mid-depth sulphidic zone and the relatively shallow chemocline separating oxic surface water and anoxic deep water with a decreased nitrate reservoir.

https://doi.org/10.1017/S0016756817000115 Published online by Cambridge University Press

Basin was stratified, with oxygenated surface seawater overlying ferruginous deep seawater. The $\delta^{15}N_{bulk}$ values of the studied samples in this interval vary from −1.2 ‰ to 3.5 ‰. The high value of 3.5 ‰ indicates that primary producers may have assimilated nitrogen from the seawater nitrate reservoir, and thus the photic zone may have been oxic or dysoxic with a relatively deep chemocline. Meanwhile, the nitrate reservoir may have been not very large, and the nitrogen sources of phytoplankton may have been both nitrate and ammonium under conditions of equilibrium among nitrogen assimilation, N_2 fixation and denitrification (Cremonese *et al.* 2013). In summary, the deep seawater in the Yangtze shelf margin area was anoxic or ferruginous, while the surface seawater was oxic or dysoxic during the Cambrian Fortunian and lower Stage 2, as shown schematically in Figure 6A.

5.c.2. Upper Stage 2 and lower Stage 3 (Interval II)

This interval features a polymetallic sulphide-rich layer that was deposited from the mid-depth zone of sulphidic seawater on the shelf margin, sandwiched between oxic surface water and ferruginous deep water, produced by MSR due to an increasing sulphate supply, possibly from continental weathering as a result of increased riverine sulphate input (Guo *et al.* 2007; Lehmann *et al.* 2007; Xu *et al.* 2012; Och *et al.* 2013; Feng *et al.* 2014; Li *et al.* 2015). Some of the studied samples in this interval show high molybdenum concentrations (>100 ppm) and low $\delta^{34}S_{py}$ (<−15 ‰), which is consistent with this sulphidic zone developed in the basin connecting well with the open ocean and enhanced oxygenation of the global ocean inferred from data of other redox proxies such as Mo isotopes (Chen *et al.* 2015).

This interval has the lowest $\delta^{15}N_{bulk}$ value (−3.2 ‰) of the studied core section. Such a low $\delta^{15}N_{bulk}$ value in the sediments may have occurred due to several potential mechanisms. One possible mechanism is that the primary producers in the shelf margin assimilated ^{15}N-depleted NH_4^+ upwelling from anoxic deep seawater where the nitrogen reservoir was dominated by NH_4^+ (Higgins *et al.* 2012). The upwelling anoxic seawater following a widespread transgression event in the early Cambrian (Steiner *et al.* 2001) may also have driven shallowing of the chemocline. Another potential mechanism is that the photic zone became anoxic or euxinic due to a rise of the chemocline, and thus N_2 fixation prevailed through green or purple sulphur bacteria, resulting in the large nitrogen isotopic fractionation during azofication (Ohkouchi *et al.* 2005; Cremonese *et al.* 2013). Different nitrogenases also had varying influences on nitrogen isotopic compositions of organisms. Zhang *et al.* (2014) reported that diazotrophs using molybdenum nitrogenases would produce very small nitrogen isotope fractionation, but vanadium-only or iron-only nitrogenases would produce fixed nitrogen with significantly lower $\delta^{15}N$ (−6 to −7 ‰), resulting in the low $\delta^{15}N$ (<−2 ‰) recorded in sediments. In euxinic seawater, molybdenum precipitates rapidly in sediments with sulphides and organic matter, decreasing the concentration of molybdenum in the local seawater significantly, especially in a restricted marine environment (Scott *et al.* 2008; Reinhard *et al.* 2013). Meanwhile, vanadium concentration is lowered as well, although not as much as the decreasing extent of molybdenum; thus, there is still reactive vanadium in the euxinic seawater (Emerson & Huested, 1991). In contrast, anoxic conditions generally tend to increase iron bioavailability, as Fe (II)-sulphides are more soluble than Fe (III)-oxides. Therefore, euxinic conditions would be favourable to V- and/or Fe- nitrogenases as important N_2-fixed enzymes rather than Mo-nitrogenases, resulting in large nitrogen isotope fractionations (Anbar & Knoll, 2002; Zhang *et al.* 2014). The significantly low $\delta^{15}N_{bulk}$ in this interval is probably the end product of all these factors. The above data and discussion suggest a decrease of the seawater oxygenation in the local Yangtze shelf margin area in the period of the upper Cambrian Stage 2 and lower Stage 3, caused by an enhancement in the MSR process as a result of increasing local marine sulphate concentration, evidenced by the decrease of $\delta^{34}S_{py}$ values noted above (Table 3). The black shales at the top of Interval II show low Mo concentrations, $\delta^{34}S_{py}$ values of 0–5 ‰ and $\delta^{15}N_{bulk}$ values between +1 ‰ and +2 ‰. These data indicate recession of the previous euxinic seawater and a return to anoxic (ferruginous) conditions of the local marine environment after lower Cambrian Stage 3.

5.c.3. Middle and upper Stage 3 (Interval III)

Geochemical data of the studied samples in the middle and upper Cambrian Stage 3 (Interval III) indicate that a widespread euxinic marine environment gradually shrank with the regression, which is supported by Feng *et al.* (2014) and Jin *et al.* (2014). Both Mo and U concentrations of the samples in this interval are much lower than those in Interval II, suggesting an anoxic but not euxinic marine environment on the slope zone of the Yangtze shelf margin. The $\delta^{15}N_{bulk}$ values of the samples in this interval vary from +1.7 ‰ to −1.7 ‰ with a descending trend from the middle to the upper Jiumenchong Formation, which probably reflects the decrease of the nitrate reservoir and the falling oxygenation level of the Yangtze shelf-margin area in this period. With consumption of the local marine nitrate reservoir due to the preceding euxinic event during the upper Cambrian Stage 2 and lower Stage 3, the nitrogen sources used by organisms in the middle and upper Cambrian Stage 3 would be mainly from atmospheric N_2 through azofication or partly from ammonium from the deep seawater, resulting in the low $\delta^{15}N_{bulk}$ values in this period compared with those of the Cambrian Fortunian and lower Stage 2. Meanwhile, TOC and TN contents in this period also appear in a decreasing trend, probably reflecting reduction of primary production and nitrogen assimilation in the shelf margin as a

https://doi.org/10.1017/S0016756817000115 Published online by Cambridge University Press

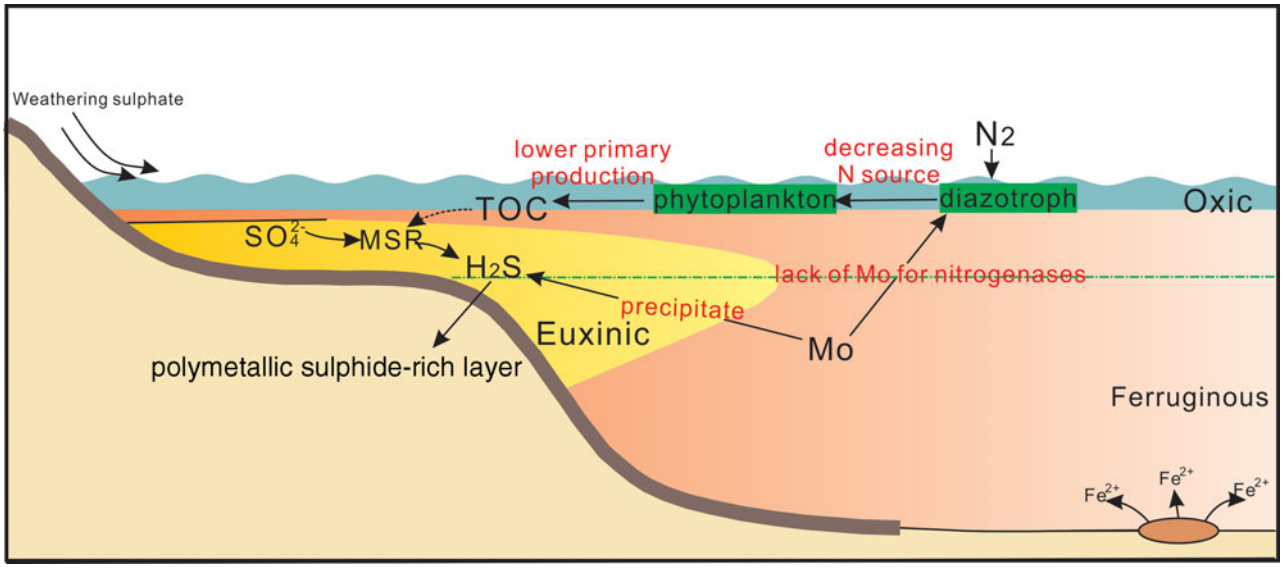

Figure 7. Schematic depiction for the biogenic negative feedback on seawater redox in the Yangtze shelf margin area. Stratified marine redox model is based on Li *et al.* (2015).

result of the low N_2-fixation efficiency. In the period after the lower Cambrian Stage 3, sea level fluctuated frequently (Haq & Schutter, 2008). With probably an event of sea level fall after the transgression in the lower Cambrian Stage 3 (Interval II), the chemocline shifted below the photic zone. Nevertheless, the anoxic zone on the Yangtze shelf margin in this period was larger than that in the Cambrian Fortunian and lower Stage 2, which possibly resulted from an increase of the restriction extent of the Nanhua Basin with the regression. The decreasing trend of $\delta^{15}N_{bulk}$ from the middle to the upper Cambrian Stage 3 (Interval III) may have been caused by enhancement of the anoxic extent of the Yangtze shelf margin area as another local anoxic event in this period (D. Wang *et al.* 2015), which may have resulted in the extinction of Niutitang sponge biota at Cambrian Stage 3 (Zhu *et al.* 2007). However, the redox state levels of marine environments in other regions than the Yangtze shelf margin and of the global ocean in the period of the Cambrian middle to upper Stage 3 require further study in the future.

5.d. Possible link between ocean geochemical cycles and biological evolution

Phosphorus and nitrogen are both essential nutrients for living organisms. Because of the enhanced marine P reservoir in the terminal Neoproterozoic, the previously P-limited marine environment may have transformed into a N-limited marine environment in the early Cambrian (e.g. Kikumoto *et al.* 2014). Biogenic nitrogen fixation provides the main input of nitrogen for the Earth ecosystem, and metallic ions of Mo, Fe and V are essential for the nitrogenases. In euxinic and ferruginous environments with very low Mo concentrations in seawater, vanadium and iron 'alternative' nitrogenases produce fixed nitrogen with significantly lower $\delta^{15}N_{bulk}$ than that produced by molybdenum nitrogenases in oxic and suboxic environments (Zhang *et al.* 2014). The production efficiency of N_2 fixation by vanadium or iron nitrogenases is also much lower than that by molybdenum nitrogenases. Recent laboratory experimental results indicate that when Mo concentration is below ~5 % of the present Mo concentration in the ocean, the rate of N_2 fixation in cultured cyanobacteria begins to decrease (Zerkle *et al.* 2006). Efficient molybdenum precipitation in euxinic seawater reduces molybdenum concentration in local seawater and thus reduces the N_2 fixation rate, causing a decrease of primary production and consequently a decrease of TN and TOC in sediments. This bioinorganic bridge linking Mo to N bioavailability would act as a negative feedback (Fig. 7) limiting the spatial and temporal extent of euxinic conditions because the bacterially mediated reduction of sulphate to sulphide would be depressed by the decrease of organic matter (Scott *et al.* 2008). After temporary euxinic conditions (upper Cambrian Stage 2 and lower Stage 3), the seawater of the Yangtze shelf margin returned to anoxic or ferruginous (middle and upper Stage 3). As hydrogen sulphide was pernicious to aerobic respiration, the transition from sulphidic to ferruginous deep seawater detoxified the basin margin, providing expanded opportunities for eukaryote diversification. The Cambrian Explosion may have benefited from such an environmental transition occurring in the Nanhua Basin as a representative in the global ocean in the early Cambrian (e.g. Chengjiang biota or Niutitang sponge biota).

6. Summary and conclusions

Trace elements, sulphur isotopes and nitrogen isotopes of the Daotuo drill core samples (the upper Liuchapo Formation and the entire Jiumenchong Formation) in

https://doi.org/10.1017/S0016756817000115 Published online by Cambridge University Press

Songtao County, NE Guizhou Province, were analysed to reconstruct the marine environmental and biological evolution of the Yangtze shelf margin during the early Cambrian. Redox conditions varied among three intervals during the period from the early Cambrian Fortunian to Stage 3 (Fig. 3). Seawater became sulphidic through microbial sulphur reduction (MSR), and the photic zone was anoxic, even euxinic, in the upper Stage 2 and lower Stage 3. Seawater returned to anoxic or ferruginous conditions after the recession of sulphidic conditions in the middle and upper Stage 3. These processes were recorded and reflected by molybdenum and uranium concentrations, sulphur isotopes and nitrogen isotopes. Furthermore, decreasing $\delta^{15}N_{bulk}$ values in the middle and upper Stage 3 suggest a gradually shrinking local marine nitrate reservoir in this period, which probably reflected the oxygenation level of the Yangtze shelf margin area falling in this period. The change of marine environment may have exerted significant influence on biological activity, affecting the nitrogen cycle in the Yangtze shelf margin area, as recorded by nitrogen isotopes in the bulk samples. Meanwhile, biological activity may also have had significant negative feedback on the local sulphidic seawater. The sulphidic seawater during the early Cambrian upper Stage 2 decayed partly due to depression in primary production as a result of the rapid deposition of molybdenum and the consequent decrease of N_2 fixation efficiency. In addition to biological activity, the change of marine redox environments between anoxic (ferruginous) and euxinic (sulphidic) conditions might be related to other factors, such as fluctuation of sea level and continental weathering flux; thus, the connections between the redox state levels of the marine environment and these factors merit further study in the future.

Acknowledgements. We thank Nina Zhao and Fuqiang Shi for assistance with the field work; Prof. Zhaohui Zhang and Qian Liu for chemical analyses; and Prof. Thomas J. Algeo and Prof. Chao Li for helpful suggestions. This study was funded by the National Basic Research Program of China (2013CB835004) and a National Natural Science Foundation of China (NSFC) program (41230102).

References

Ader, M., Sansjofre, P., Halverson, G. P., Busigny, V., Trindade, R. I. F., Kunzmann, M. & Nogueira, A. C. R. 2014. Ocean redox structure across the Late Neoproterozoic Oxygenation Event: a nitrogen isotope perspective. *Earth and Planetary Science Letters* **396**, 1–13.

Algeo, T. J., Luo, G. M., Song, H. Y., Lyons, T. W. & Canfield, D. E. 2015. Reconstruction of secular variation in seawater sulfate concentrations. *Biogeosicences* **12**(7), 2131–51.

Algeo, T. J. & Lyons, T. W. 2006. Mo–total organic carbon covariation in modern anoxic marine environments: implications for analysis of paleoredox and paleohydrographic conditions. *Paleoceanography* **21**(1), PA1016. doi: 10.1029/2004PA001112.

Algeo, T. J. & Rowe, H. 2012. Paleoceanographic applications of trace-metal concentration data. *Chemical Geology* **324–325**, 6–18.

Algeo, T. J. & Tribovillard, N. 2009. Environmental analysis of paleoceanographic systems based on molybdenum–uranium covariation. *Chemical Geology* **268**(3–4), 211–25.

Anbar, A. D. & Knoll A., H. 2002. Proterozoic ocean chemistry and evolution: a bioinorganic bridge? *Science* **297**(5584), 1137–42.

Berner, E. K. & Berner, R. 1996. *Global environment: water, air and geochemical cycles*. Upper Saddle River, NJ: Prentice Hall, 376 pp.

Calvert, S. 2004. Beware intercepts: interpreting compositional ratios in multi-component sediments and sedimentary rocks. *Organic Geochemistry* **35**, 981–7.

Canfield, D. E. 2001. Biogeochemistry of sulfur isotopes. *Stable Isotope Geochemistry* **43**, 607–36.

Canfield, D. E. 2004. The evolution of the earth surface sulfur reservoir. *American Journal of Science* **304**, 839–61.

Canfield, D. E. 2005. The early history of atmospheric oxygen: homage to Robert M. Garrels. *Annual Review of Earth and Planetary Sciences* **33**, 1–36.

Canfield, D. E., Poulton, S. W. & Narbonne, G. M. 2007. Late-Neoproterozoic deep-ocean oxygenation and the rise of animal life. *Science* **315**(5808), 92–5.

Chen, X., Ling, H. F., Vance, D., Shields-Zhou, G. A., Zhu, M. Y., Poulton, S. W., Och, L. M., Jiang, S. Y., Li, D., Cremonese, L. & Archer, C. 2015. Rise to modern levels of ocean oxygenation coincided with the Cambrian radiation of animals. *Nature Communications* **6**, 7142. doi: 10.1038/ncomms8142.

Cheng, M., Li, C., Zhou, L., Algeo, T. J., Zhang, F. F., Romaniello, S., Jin, C. S., Lei, L. D., Feng, L. J. & Jiang, S. Y. 2016. Marine Mo biogeochemistry in the context of dynamically euxinic mid-depth waters: a case study of the lower Cambrian Niutitang shales, South China. *Geochimica et Cosmochimica Acta* **183**, 79–93.

Cremonese, L., Shields-Zhou, G., Struck, U., Ling, H.-F., Och, L., Chen, X. & Li, D. 2013. Marine biogeochemical cycling during the early Cambrian constrained by a nitrogen and organic carbon isotope study of the Xiaotan section, South China. *Precambrian Research* **225**, 148–65.

Emerson, S. R. & Huested, S. S. 1991. Ocena anoxia and the concentrations of molybdenum and vanadium in seawater. *Marine Chemistry* **34**(34): 177–96.

Feng, L., Li, C., Huang, J., Chang, H. & Chu, X. 2014. A sulfate control on marine mid-depth euxinia on the early Cambrian (ca.529–521Ma) Yangtze platform, South China. *Precambrian Research* **246**, 123–33.

Fike, D. A., Grotzinger, J. P., Pratt, L. M. & Summons, R. E. 2006. Oxidation of the Ediacaran ocean. *Nature* **444**(7120), 744–7.

Godfrey, L. V. & Falkowski, P. G. 2009. The cycling and redox state of nitrogen in the Archaean ocean. *Nature Geoscience* **2**(10), 725–9.

Goldberg, E. D. 1963. Mineralogy and chemistry of marine sedimentation. In *Submarine Geology* (ed. F. P. Shepard), pp. 436–66. New York: Harper and Row.

Goldberg, T., Poulton, S. & Strauss, H. 2005. Sulfur and oxygen isotope signatures of late Neoproterozoic to early Cambrian sulfate, Yangtze Platform, China: diagenetic constraints and seawater evolution. *Precambrian Research* **137**(3–4), 223–41.

Goldberg, T., Strauss, H., Guo, Q. & Liu, C. 2007. Reconstructing marine redox conditions for the Early Cambrian Yangtze Platform: evidence from biogenic sulfur

and organic carbon isotopes. *Palaeogeography Palaeoclimatology Palaeoecology* **254**(1–2), 175–93.

Guo, Q., Shields, G. A., Liu, C., Strauss, H., Zhu, M., Pi, D., Goldberg, T. & Yang, X. 2007. Trace element chemostratigraphy of two Ediacaran–Cambrian successions in South China: implications for organosedimentary metal enrichment and silicification in the Early Cambrian. *Palaeogeography, Palaeoclimatology, Palaeoecology* **254**(1–2), 194–216.

Habicht, K. S., Gade, M., Thamdrup, B., Berg, P. & Canfield, D. E. 2002. Calibration of sulfate levels in the Archean ocean. *Science* **298**, 2372–4.

Habicht, K. S., Salling, L., Thamdrup, B. & Canfield, D. E. 2005. Effect of low sulfate concentrations on lactate oxidation and isotope fractionation during sulfate reduction by Archaeoglobus fulgidus strain Z†. *Applied and Environmental Microbiology* **71**(7), 3770–7.

Haq, B. U. & Schutter, S. R. 2008. A chronology of Paleozoic sea-level changes. *Science* **322** (5898), 64–8.

Harrison, A. G. & Thode, H. G. 1958. Mechanism of the bacterial reduction of sulfate from isotope fractionation studies. *Transactions of the Faraday Society* **54**, 84–92.

Higgins, M. B., Robinson, R. S., Husson, J. M., Carter, S. J. & Pearson, A. 2012. Dominant eukaryotic export production during ocean anoxic events reflects the importance of recycled NH_4^+. *Proceedings of the National Academy of Sciences of the United States of America* **109**, 2269–74.

Holland, H. D. 2006. The oxygenation of the atmosphere and oceans. *Philosophical Transactions of the Royal Society B Biological Sciences* **361**(1470), 903–15.

Holser, W., Schidlowski, M., Mackenzie, F. & Maynard, J. 1988. Biogeochemical cycles of carbon and sulfur. *Chemical Cycles in the Evolution of the Earth*. Chichester: John Wiley & Sons, 105–74.

Jiang, S., Chen, Y., Ling, H., Yang, J., Feng, H. & Ni, P. 2006. Trace- and rare-earth element geochemistry and Pb–Pb dating of black shales and intercalated Ni–Mo–PGE–Au sulfide ores in Lower Cambrian strata, Yangtze Platform, South China. *Mineralium Deposita* **41**(5), 453–467.

Jin, C. S., Li, C., Algeo, T. J., Planavsky, N. J., Cui, H., Yang, X. L., Zhao, Y. L., Zhang, X. L. & Xie, S. C. 2016. A highly redox-heterogeneous ocean in South China during the Early Cambrian (~529–514 Ma): implications for a local "Cambrian Explosion". *Earth and Planetary Science Letters* **441**, 38–51.

Jin, C. S., Li, C., Peng, X. F., Cui, H., Shi, W., Zhang, Z.H., Luo, G. M. & Xie, S. C. 2014. Spatiotemporal variability of ocean chemistry in the early Cambrian, South China. *Science China Earth Science* **57**, 579–91.

Jones, D. S. & Fike, D. A. 2013. Dynamic sulfur and carbon cycling through the end-Ordovician extinction revealed by paired sulfate-pyrite $\delta^{34}S$. *Earth and Planetary Science Letters* **363**, 144–55.

Kikumoto, R., Tahata, M., Nishizawa, M., Sawaki, Y., Maruyama, S., Shu, D.G., Han, J., Komiya, T., Takai, K. & Ueno, Y. 2014. Nitrogen isotope chemostratigraphy of the Ediacaran and Early Cambrian platform sequence at Three Gorges, South China. *Gondwana Research* **25**, 1057–69.

Lehmann, B., Nägler, T. F., Holland, H. D., Wille, M., Mao, J., Pan, J., Ma, D. & Dulski, P. 2007. Highly metalliferous carbonaceous shale and Early Cambrian seawater. *Geology* **35**(5), 403–6.

Li, C., Cheng, M., Algeo, T. J. & Xie, S. C. 2015. A theoretical prediction of chemical zonation in early oceans (>520 Ma). *Science in China D (Earth Sciences)* **58**(11), 1901–9.

Li, C., Love, G. D., Lyons, T. W., Fike, D. A., Sessions, A. L. & Chu, X. 2010. A stratified redox model for the Ediacaran ocean. *Science* **328**(5974), 80–3.

Li, C., Love, G. D., Lyons, T. W., Scott, C. T., Feng, L., Huang, J., Chang, H., Zhang, Q. & Chu, X. 2012. Evidence for a redox stratified Cryogenian marine basin, Datangpo Formation, South China. *Earth and Planetary Science Letters* **331–332**, 246–56.

Li, Z., Bogdanova, S. V., Collins, A. S., Davidson, A., De Waele, B., Ernst, R. E., Fitzsimons, I. C. W., Fuck, R. A., Gladkochub, D. P., Jacobs, J., Karlstrom, K. E., Lu, S., Natapov, L. M., Pease, V., Pisarevsky, S. A., Thrane, K. & Vernikovsky, V. 2008. Assembly, configuration, and break-up history of Rodinia: a synthesis. *Precambrian Research* **160**(1–2), 179–210.

Ling, H.-F., Chen, X., Li, D., Wang, D., Shields-Zhou, G. A. & Zhu, M. 2013. Cerium anomaly variations in Ediacaran – earliest Cambrian carbonates from the Yangtze Gorges area, South China: implications for oxygenation of coeval shallow seawater. *Precambrian Research* **225**, 110–27.

Lyons, T. W., Anbar, A. D., Severmann, S., Scott, C. & Gill, B. C. 2009. Tracking Euxinia in the ancient ocean: a multiproxy perspective and proterozoic case study. *Annual Review of Earth and Planetary Sciences* **37**(1), 507–34.

Lyons, T. W., Reinhard, C. T. & Planavsky, N. J. 2014. The rise of oxygen in Earth's early ocean and atmosphere. *Nature* **506**(7488), 307–15.

Och, L. M. & Shields-Zhou, G. A. 2012. The Neoproterozoic oxygenation event: environmental perturbations and biogeochemical cycling. *Earth-Science Reviews* **110**(1–4), 26–57.

Och, L. M., Shields-Zhou, G. A., Poulton, S. W., Manning, C., Thirlwall, M. F., Li, D., Chen, X., Ling, H., Osborn, T. & Cremonese, L. 2013. Redox changes in Early Cambrian black shales at Xiaotan section, Yunnan Province, South China. *Precambrian Research* **225**, 166–89.

Ohkouchi, N., Nakajima, Y., Okada, H., Ogawa, N. O., Suga, H., Oguri, K. & Kitazato, H. 2005. Biogeochemical processes in the saline meromictic Lake Kaiike, Japan: implications from molecular isotopic evidences of photosynthetic pigments. *Environmental Microbiology* **7**, 1009–16.

Pinti, D. L., Hashizume, K., Orberger, B., Gallien, J. P., Cloquet, C. & Massault, M. 2007. Biogenic nitrogen and carbon in Fe-Mn-oxyhydroxides from an Archean chert, Marble Bar, Western Australia. *Geochemistry, Geophysics, Geosystems* **8**, Q02007. doi: 10.1029/2006GC001394.

Piper, D. Z. & Calvert, S. E. 2009. A marine biogeochemical perspective on black shale deposition. *Earth-Science Reviews* **95** (1–2), 63–96.

Prokopenko, M., Hammond, D., Berelson, W., Bernhard, J., Stott, L., Douglas, R. 2006. Nitrogen cycling in the sediments of Santa Barbara basin and Eastern Subtropical North Pacific: nitrogen isotopes, diagenesis and possible chemosymbiosis between two lithotrophs (Thioploca and Anammox) – 'riding on a glider'. *Earth and Planetary Science Letters* **242**, 186–204.

Redfield, A. C. 1963. The influence of organisms on the composition of seawater. In *The Sea* (ed. M. N. Hill), vol. II, pp. 26–77. New York: John Wiley.

Reinhard, C. T., Planavsky, N. J., Robbins, L. J., Partin, C. A., Gill, B. C., Lalonde, S. V., Bekker, A.,

Konhauser, K. O. & Lyons, T. W. 2013. Proterozoic ocean redox and biogeochemical stasis. *Proceedings of the National Academy of Sciences of the United States of America* **110**(14), 5357–62.

Sahoo, S. K., Planavsky, N. J., Kendall, B., Wang, X., Shi, X., Scott, C., Anbar, A. D., Lyons, T. W. & Jiang, G. 2012. Ocean oxygenation in the wake of the Marinoan glaciation. *Nature* **489**(7417), 546–9.

Scott, C. & Lyons, T. W. 2012. Contrasting molybdenum cycling and isotopic properties in euxinic versus non-euxinic sediments and sedimentary rocks: refining the paleoproxies. *Chemical Geology* **324–325**, 19–27.

Scott, C., Lyons, T. W., Bekker, A., Shen, Y., Poulton, S. W., Chu, X. & Anbar, A. D. 2008. Tracing the stepwise oxygenation of the Proterozoic ocean. *Nature* **452**(7186), 456–59.

Shen, Y., Zhao, R., Chu, X. & Lei, J. 1998. The carbon and sulfate isotope signature in the Precambrian–Cambrian transition series of the Yangtze Platform. *Precambrian Research* **89**, 77–86.

Shields-Zhou, G. & Zhu, M. 2013. Biogeochemical changes across the Ediacaran–Cambrian transition in South China. *Precambrian Research* **225**, 1–6.

Sigman, D., Karsh, K. & Casciotti, K. 2009. Ocean process tracers: nitrogen isotopes in the ocean. *Encyclopedia of Ocean Science*, 2nd edn. Amsterdam: Elsevier.

Steiner, M., Zhu, M., Weber, B. & Geyer, G. 2001. The Lower Cambrian of eastern Yun-nan: trilobite-based biostratigraphy and related faunas. *Acta Palaeontologica Sinica* **40** (Suppl.), 63–79.

Strauss, H. 1997. The isotopic composition of sedimentary sulfur through time. *Palaeogeography, Palaeoclimatology, Palaeoecology* **132**, 97–118.

Strauss, H. 1999. Geological evolution from isotope proxy signals – sulfur. *Chemical Geology*, **161**(1–3), 89–101.

Taylor, S. R. & McLennan, S. M. 1985. *The Continental Crust: Its Composition and Evolution*. Oxford: Blackwell.

Thomazo, C., Ader, M. & Philippot, P. 2011. Extreme ^{15}N-enrichments in 2.72-Gyrold sediments: evidence for a turning point in the nitrogen cycle. *Geobiology* **9**,107–20.

Tribovillard, N., Algeo, T. J., Baudin, F. & Riboulleau, A. 2012. Analysis of marine environmental conditions based on molybdenum uranium covariation: applications to Mesozoic paleoceanography. *Chemical Geology* **324–325**, 46–58.

Tribovillard, N., Algeo, T. J., Lyons, T. & Riboulleau, A. 2006. Trace metals as paleoredox and paleoproductivity proxies: an update. *Chemical Geology* **232**(1–2), 12–32.

Wang, D., Ulrich, S., Ling, H-F., Guo, Q-J., Shields-Zhou, G. A., Zhu, M-Y. & Yao, S-P. 2015. Marine redox variations and nitrogen cycle of the early Cambrian southern margin of the Yangtze Platform, South China: evidence from nitrogen and organic carbon isotopes. *Precambrian Research* **267**, 209–26.

Wang, X., Shi, X., Jiang, G. & Zhang, W. 2012. New U–Pb age from the basal Niutitang Formation in South China: implications for diachronous development and condensation of stratigraphic units across the Yangtze platform at the Ediacaran–Cambrian transition. *Journal of Asian Earth Sciences* **48**, 1–8.

Wang, X., Shi, X., Zhao, X. & Tang, D. 2015. Increase of seawater Mo inventory and ocean oxygenation during the early Cambrian. *Palaeogeography Palaeoclimatology Palaeoecology* **440**, 621–31.

Wedepohl, K. H. 1995. The composition of the continental crust. *Geochimica et Cosmochimica Acta* **59**, 1217–32.

Wei, W., Wang, D., Li, D., Ling, H. F., Chen, X., Wei, G. Y., Zhang, F. F., Zhu, X. K. & Yan, B. 2016. Evidence from nitrogen isotopes and Mo contents of the Basal Datangpo Formation, northeastern Guizhou, South China. *Journal of Earth Science* **27**(2), 233–41.

Xu, L. G., Lehmann, B., Mao, J. W., Nägler, T. F., Neubert, N., Böttcher, M. E. & Escher, P. 2012. Mo isotope and trace element patterns of Lower Cambrian black shales in South China: multi-proxy constraints on the paleoenvironment. *Chemical Geology* **318–319**, 45–59.

Xu, L. G., Lehmann, B., Mao, J. W., Qu, W. J. & Du, A. D. 2011. Re–Os age of polymetallic Ni-Mo-PGE-Au mineralization in Early Cambrian black shales of South China – a reassessment. *Economic Geology* **106**, 511–22.

Zerkle, A. L., House, C. H., Cox, R. P. & Canfield, D. E. 2006. Metal limitation of cyanobacterial N_2 fixation and implications for the Precambrian nitrogen cycle. *Geobiology* **4**, 285–97.

Zerkle, A. L., Junium, C. K., Canfield, D. E. & House, C. H. 2008. Production of ^{15}N-depleted biomass during cyanobacterial N_2-fixation at high Fe concentrations. *Journal of Geophysical Research – Biogeosciences* **113** (G3). doi: 10.1029/2007JG000651.

Zhang, X. N., Sigman, D. M., Morel, F. M. M. & Kraepiel, A. M. L. 2014. Nitrogen isotope fractionation by alternative nitrogenases and past ocean anoxia. *Proceedings of the National Academy of Sciences of the United States of America* **111**(13), 4782–7.

Zhu, M., Strauss, H. & Shields, G. A. 2007. From snowball earth to the Cambrian bioradiation: calibration of Ediacaran-Cambrian earth history in South China. *Palaeogeography, Palaeoclimatology, Palaeoecology* **254**, 1–6.

Zhu, M., Zhang, J., Steiner, M., Yang, A., Li, G. & Erdtmann, B. D. 2003. Sinian-Cambrian stratigraphic framework for shallow- to deep-water environments of the Yangtze Platform: an integrated approach. *Progress in Natural Science* **13**, 951–60.

https://doi.org/10.1017/S0016756817000115 Published online by Cambridge University Press